A cytoskeletal-based perimeter fence selectively corrals a sub-population of cell surface Kv2.1 channels

Michael M. Tamkun[1,2,*], Kristen M. S. O'Connell[1] and Annah S. Rolig[2]

[1]Department of Biomedical Sciences and [2]Department of Biochemistry and Molecular Biology, Colorado State University, Ft. Collins, CO 80523, USA

*Author for correspondence (e-mail: tamkunmm@lamar.colostate.edu)

Accepted 9 May 2007
Journal of Cell Science 120, 2413-2423 Published by The Company of Biologists 2007
doi:10.1242/jcs.007351

Summary

The Kv2.1 delayed-rectifier channel trafficks to 1-3 μm^2 clusters on the surface of neurons and transfected HEK cells. Single quantum dot (Qdot) tracking and FRAP approaches were used to quantify the diffusion of GFP-labeled Kv2.1 channels on the cell surface and address the mechanisms underlying the formation of these unique membrane structures. Mean square displacement analysis of single Kv2.1 channel tracks inside or outside the surface clusters yielded mean diffusion coefficients of 0.03±0.02 μm^2/second and 0.06±0.05 μm^2/second, respectively. Kv2.1 channels outside the clusters effectively ignore the cluster boundary, readily diffusing through these microdomains. However, in 5% of the tracks analyzed, single, non-clustered channels were observed to cross into a cluster and become corralled within the cluster perimeter. Alexa Fluor 594-labelled phalloidin staining and mCherry-Kv2.1 co-expression with GFP-actin indicated that the Kv2.1 surface clusters form where the cortical actin cytoskeleton is reduced. Kv2.1 channels lacking the C-terminus do not form clusters, freely diffusing over the cell surface with a mean diffusion coefficient of 0.07±0.04 μm^2/second. These data support a model whereby the Kv2.1 clusters are formed by sub-membrane cytoskeletal structures that limit the lateral diffusion of only the sub-population of Kv2.1 channels carrying the appropriate modifications on the Kv2.1 C-terminus.

Supplementary material available online at
http://jcs.biologists.org/cgi/content/full/120/14/2413/DC1

Key words: Cytoskeletal fence, Fluorescence, Live cell imaging, Localization, Potassium channel, Quantum dot tracking

Introduction

Voltage-gated K^+ (Kv) channels play a key role in establishing the resting membrane potential, shaping action potential repolarization and regulating spike frequency in many cell types. These channels often target specific plasma membrane regions where they probably assemble into signaling complexes. However, in most cases little is known about the mechanisms responsible for this localization, even though the modulation of voltage-gated ion channel surface expression and localization probably represents a central mechanism in the regulation of cellular excitability. Given the central role that the Kv2.1 delayed rectifier plays in neurons (Du et al., 2000; Misonou et al., 2005b), the heart (Nerbonne, 2000), pancreatic β cells (Tamarina et al., 2005) and vascular smooth muscle (Coppock et al., 2001), a greater understanding of the mechanisms regulating its surface localization is essential.

As originally noted by Trimmer and colleagues (Scannevin et al., 1996), Kv2.1 is expressed primarily in the somato-dendritic region of hippocampal neurons where it is found in cell surface clusters that often colocalize with ryanodine receptors and sarcoplasmic reticulum-like sub-surface cisterns (Antonucci et al., 2001; Du et al., 1998). Similar clusters also form upon expression of Kv2.1 in HEK cells (O'Connell and Tamkun, 2005), probably owing to the fact that HEK cells are likely to be of neuronal origin (Shaw et al., 2002). In both hippocampal neurons and transfected HEK cells, glutamate or carbachol treatment induces dephosphorylation and Kv2.1 declustering (Misonou et al., 2005a; Misonou et al., 2004; Mohapatra and Trimmer, 2006). Both treatments also result in a 20 mV hyperpolarizing shift in the activation curve for I_K. Chemically induced ischemia also induces declustering, dephosphorylation, and the hyperpolarizing shift in the midpoint of activation (Misonou et al., 2005a; Mohapatra and Trimmer, 2006). These data suggest a strong link between cluster formation, channel phosphorylation, and the voltage-dependence of activation. The increase in channel activity that is linked to declustering may be a neuroprotective response to hypoxia or ischemic insult (Misonou et al., 2005b). However, it should be noted that Kv2.1 trafficking to the cell surface has also been implicated in cortical neuron apoptosis (Pal et al., 2003; Pal et al., 2006).

The clustering of cell surface proteins is routinely assumed to be due to relatively static interactions with scaffolding proteins that in turn are attached to cytoskeletal components. However, our previous work (O'Connell et al., 2006) indicated that although these Kv2.1-containing microdomains are stable structures on the cell surface, the channels retained within the cluster perimeter are surprisingly mobile. The mobility of the confined Kv2.1 channels within the cluster argues against a static scaffolding-based structure being responsible for the

microdomain. Kv2.1-containing surface domains also appear to be specialized sites for Kv2.1 insertion as they acquire channel from Kv2.1-containing intracellular transport vesicles (O'Connell et al., 2006). Thus, these Kv2.1-containing cell surface structures probably allow for the efficient trafficking to and from the cell surface while at the same time potentially sequestering channel with signaling proteins that regulate channel function.

The present study had several goals, all related to understanding the cluster-forming mechanism. The first was to quantify the lateral diffusion of Kv2.1 inside and outside the surface cluster. If a true fence forms the cluster, as opposed to transient interactions with scaffolding proteins, the diffusion coefficients in both surface compartments should be similar; mobile and scaffolding-protein-tethered membrane proteins often have diffusion coefficients that vary by one or two orders of magnitude (Dahan et al., 2003; Meier et al., 2001; Peran et al., 2001; Sako and Kusumi, 1995; Tardin et al., 2003). The second goal was to address the question of whether other membrane proteins can cross the cluster boundary or fence. The third line of investigation involved further examination of the role that the cortical actin cytoskeleton plays in forming the fence perimeter. These data continue to support the hypothesis that a diffusion-limiting fence forms the Kv2.1 surface clusters. In addition, this fence is specific for a sub-population of mobile Kv2.1 channels – the ones corralled within the cluster. Other membrane proteins, e.g. non-clustered Kv2.1 and Kv1.4, ignore this fence and freely diffuse across it. The perimeter fence is probably formed by structures attached to the cortical cytoskeleton as opposed to elements incorporated into, or directly attached to, the plasma membrane. Although cytoskeletal elements have been proposed previously to be responsible for the restricted diffusion of membrane proteins (Kusumi et al., 2005; Kwik et al., 2003; Morone et al., 2006), this work represents the first report of the selective corralling of a membrane protein sub-population to generate stable cell surface structures, which are several micrometers in diameter.

Results

Kv2.1 channels target discrete cell surface clusters in hippocampal neurons in situ (Misonou et al., 2005a) and in transfected hippocampal neurons and HEK cells in culture (O'Connell et al., 2006; O'Connell and Tamkun, 2005). The behavior and regulation of these clusters are nearly identical in HEK cells and neurons (Misonou et al., 2005a; Mohapatra and Trimmer, 2006), indicating that HEK cells represent a reasonable model system in which to study the formation and maintenance of these unique membrane structures. Thus, we continued to use HEK cells as a model system in our present study. We have emphasized the Kv2.1 clusters on the basal HEK cell surface because this region is more amenable to continuous live cell imaging. Importantly, using antibody labeling of live cells via an extracellular HA epitope inserted into GFP-Kv2.1, we previously confirmed that the GFP-Kv2.1 fluorescence being imaged at the basal surface represents true cell surface channel (O'Connell et al., 2006).

Kv2.1 can demonstrate both a clustered and non-clustered distribution in the same HEK cell

Although wild-type Kv2.1 is normally observed within discrete surface clusters in transfected HEK cells under control conditions (Misonou et al., 2005a; Mohapatra and Trimmer, 2006; O'Connell et al., 2006; O'Connell and Tamkun, 2005), this channel can also be detected outside these surface microdomains where it is homogenously dispersed over the cell surface. Such non-clustered expression of GFP-Kv2.1 in a cell that also has the usual surface clusters is illustrated in Fig. 1. Such cells were used to measure Kv2.1 diffusion both inside and outside the surface clusters.

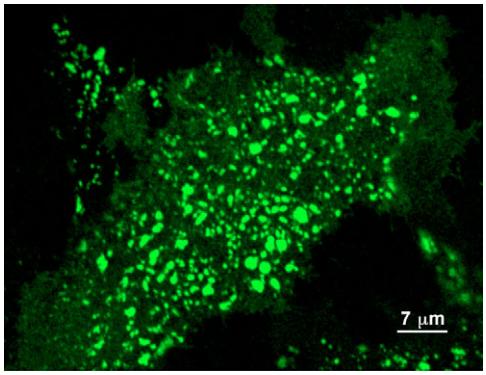

Fig. 1. GFP-Kv2.1 can show both a clustered and non-clustered distribution in HEK cells. HEK cells transfected with GFP-Kv2.1-loopBAD were imaged to detect GFP fluorescence of the GFP-Kv2.1-loopBAD expression outside the characteristic surface clusters.

Single-particle tracking of Kv2.1 channels on both sides of the cluster perimeter

We previously used quantum dot (Qdot) labeling of individual GFP-Kv2.1 surface channels to demonstrate that the channel within the cluster boundary is mobile (O'Connell et al., 2006). In our present work, this approach is used to quantify the movement of individual channels on both sides of the cluster perimeter. Fig. 2 illustrates representative, single GFP-Kv2.1-loopBAD channel trajectories that were recorded with our Qdot labeling approach. Fig. 2A shows the most common track observed in our studies. Here the Qdot track is contained entirely within the GFP-Kv2.1 cluster. Single-channel confinement often exceeded 25 minutes, which was the longest imaging period used. Single-channel diffusion within the cluster perimeter was quantified by a mean square displacement (MSD) analysis using the *x*-*y* coordinates obtained from the single Qdot tracks. Such analysis provides information on the type of diffusion and the diffusion coefficient (Kusumi et al., 2005). The shape of a MSD plot is indicative of the type of diffusion. Linear plots represent random movement, a decreasing slope indicates confinement and directed movement generates MSD plots of increasing slope. Since the stepwise data of the entire track are contained within the first few time points of the MSD plot, the initial slope of a MSD plot is directly related to the diffusion coefficient as described in the Materials and Methods.

The Qdot track of the cluster-confined channel was used to generate the MSD plot shown in the right-hand panel of Fig. 2A. Note that the decreasing slope, which is indicative of restricted diffusion, is predicted for a channel trapped within the surface cluster. Eighteen of 21 MSD plots for clustered

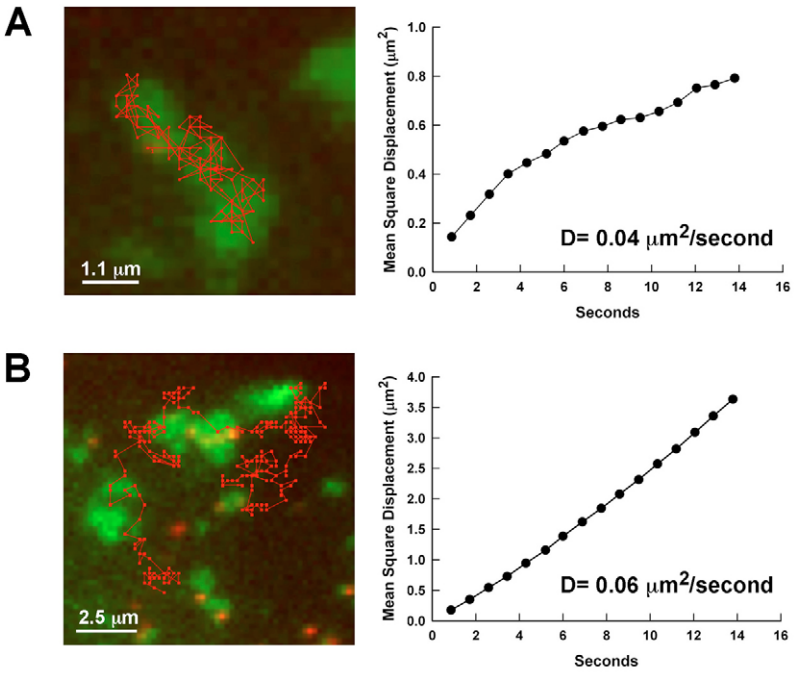

Fig. 2. Single-particle tracking of wild-type GFP-Kv2.1-loopBAD channels. HEK cells expressing GFP-Kv2.1-loopBAD were enzymatically biotinylated and then tagged at low efficiency with streptavidin-labeled 605 quantum dots as described in the Materials and Methods. The two most common classes of single Qdot tracks observed are indicated. (A) Single-particle track of a channel trapped within a cluster perimeter along with the corresponding MSD analysis of channel diffusion. In this case, a diffusion coefficient of 0.04 μm^2/second was calculated from the initial slope. Overall, MSD analysis of Kv2.1 channel movement within clusters yielded a mean diffusion coefficient of 0.03±0.02 μm^2/second, n=21. (B) Single-particle track of a channel outside the cluster whose movement was indifferent to the cluster perimeter. Analysis of the corresponding MSD plot for this track yielded a diffusion coefficient of 0.06 μm^2/second. Analysis of multiple tracks derived from non-clustered channels yielded a mean diffusion coefficient of 0.06±0.05 μm^2/second, n=33. Cells were imaged every 0.8 seconds.

channels showed this expected shape. The diffusion coefficient calculated from the initial slope of the plot in Fig. 2A was 0.04 μm^2/second. Overall, Kv2.1 channels within clusters yielded a mean diffusion coefficient of 0.03±0.02 μm^2/second, n=21, as derived from the MSD analysis.

The second most common Qdot track obtained was one illustrating the movement of a non-clustered channel across the plasma membrane as shown in Fig. 2B. This track was not influenced by the cluster perimeters; the channel transiently entered several clusters on its journey but never resided within a cluster for more than 8 seconds. This single-channel track generated the MSD plot shown in the right-hand panel of Fig. 2B. As expected, this MSD plot is relatively linear and 28/33 MSD plots for non-clustered channels were linear as expected for a particle with unrestricted diffusion. Analysis of the initial slope yielded a diffusion coefficient of 0.06 μm^2/second. Analysis of multiple tracks derived from non-clustered channels yielded a mean diffusion coefficient of 0.06±0.05 μm^2/second, n=33.

Removal of the last 318 amino acids from Kv2.1 results in a truncation mutant that fails to form surface clusters in both hippocampal neurons (Lim et al., 2000) and HEK cells as illustrated in Fig. 3A. When the single-particle-tracking MSD analysis was applied to this channel, the data illustrated in Fig. 3B,C were obtained. Here the linear shape of the MSD plot indicates random diffusion, as did 9/10 plots, and the calculated diffusion coefficient in this example was 0.10 μm^2/second. The mean diffusion coefficient was 0.07±0.04 μm^2/second, n=10.

The MSD analysis indicates that wild-type Kv2.1 channels on both sides of the cluster perimeter – inside and outside the clusters – and the non-clustering C-terminal truncation, have similar diffusion coefficients, ranging from 0.03 to 0.07 μm^2/second. Plasma membrane localization via scaffolding protein interactions often results in diffusion coefficient differences of almost two orders of magnitude between localized and non-localized proteins (see Table 1). Thus, it is most likely that Kv2.1 clustering is via a corral-forming fence as opposed to direct interactions between the channels and scaffolding proteins.

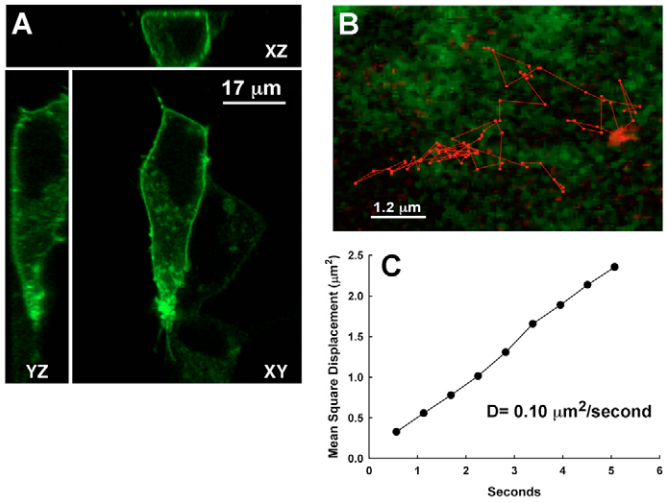

Fig. 3. Analysis of GFP-Kv2.1-loopBAD ΔC mobility on the cell surface. HEK cells expressing a GFP-Kv2.1-loopBAD channel without the C-terminal 318 amino acids (ΔC) were enzymatically biotinylated and tagged with streptavidin-labeled 655 quantum dots as described in the Materials and Methods. (A) Non-clustered cell surface distribution of this mutant channel in three dimensions. (B) The Qdot single-particle track used to generate the MSD plot indicated in C. In this case a diffusion coefficient of 0.10 μm^2/second was calculated from the initial slope. Overall the mean diffusion coefficient equalled 0.07±0.04 μm^2/second, n=10, for these mutant channels incapable of forming surface clusters. Cells were imaged every 0.55 seconds.

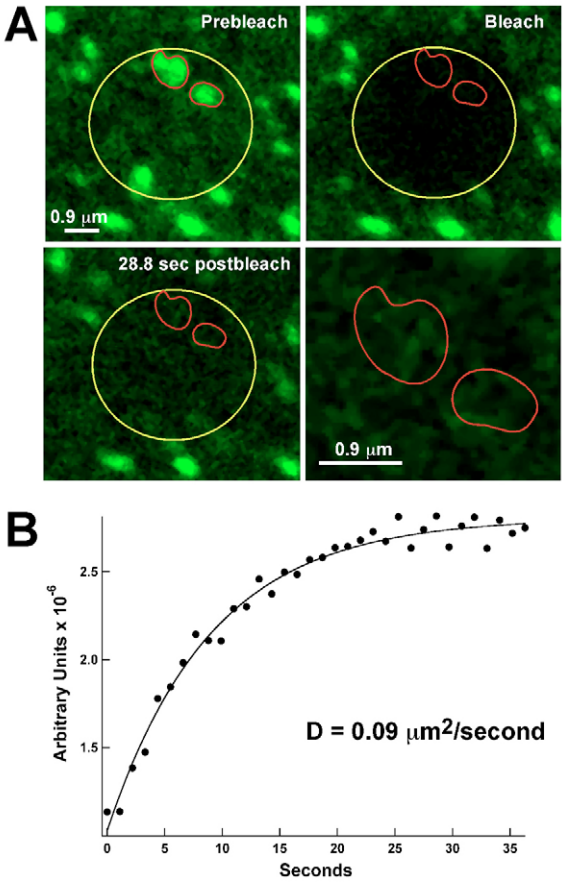

Fig. 4. FRAP analysis of Kv2.1 mobility outside the cell surface cluster. (A) Imaging of a HEK cell expressing GFP-Kv2.1 before and after photobleach within the indicated region of interest (yellow circle). Prebleach and postbleach images and the fluorescence recovery at 28.8 seconds postbleach are shown. The perimeters of the clusters observed in the prebleach image are indicated in red. Note that the fluorescence intensity within the cluster perimeter recovers to the prebleach background level over this time interval as illustrated in the lower right panel. (B) Time course of fluorescence recovery within the bleach ROI, illustrating a FRAP time constant of 9.0 seconds in this representative experiment. Using this value, we estimated that non-clustered Kv2.1 has a diffusion coefficient of 0.09 μm^2/second. The mean diffusion coefficient calculated for non-clustered channels using this approach was 0.08±0.03 μm^2/second, n=10. Cells were imaged every 1.1 seconds.

FRAP analysis demonstrates that the Kv2.1 channels outside the surface cluster readily cross the microdomain-defining perimeter

HEK cells expressing cell surface Kv2.1 in both the expected surface clusters and in the adjacent membrane were chosen for FRAP analysis. The yellow circle in Fig. 4A (Prebleach) outlines the area chosen for photobleach because it contained surface clusters. Both the GFP-Kv2.1-loopBAD inside these clusters and the homogenously distributed, non-clustered GFP-Kv2.1-loopBAD in the adjacent membrane were completely bleached following a 1-second illumination with the 405 nm laser (Fig. 4A, Bleach). The fluorescence recovery was then monitored over time, with the fluorescence observed at 28.8 seconds illustrated in Fig. 4A. As best shown by the magnified outline of the original cluster perimeters in Fig. 4A, lower right panel, recovery within the cluster did occur but only to the background level of the adjacent membrane. These results are consistent with non-clustered Kv2.1 channel crossing the cluster perimeter, thus readily diffusing into, and through, the cluster of bleached Kv2.1 channels. A cluster perimeter impermeable to non-clustered channel would be predicted to result in dark patches as the mobile, non-clustered channel is excluded during the recovery period. The short FRAP duration (<40 seconds) makes it unlikely that any of the observed recovery was due to the insertion of nascent channels into the plasma membrane.

The time course of fluorescence recovery was quantified over the entire bleach ROI as shown in Fig. 4B. The time constant for recovery in this single experiment was 9.0 seconds. Using this value and the method of Axelrod to relate the recovery time course to the diffusion coefficient (Axelrod et al., 1976), we calculated that in this experiment non-clustered Kv2.1 had a diffusion coefficient of 0.09 μm^2/second. The mean diffusion coefficient calculated for non-clustered channel using this approach was 0.08±0.03 μm^2/second, n=10; a value similar to the diffusion coefficient measured via the single particle tracking approach illustrated in Fig. 2B. In addition, the apparent indifference of the non-clustered channel to the cluster perimeter agrees with the Qdot track presented in Fig. 2B.

Kv1.4 channels readily diffuse across the Kv2.1 cluster perimeter

The data presented in Figs 2 and 4 indicate that the diffusion of Kv2.1 outside the surface clusters is unaltered by the cluster perimeter fence. To determine whether other membrane proteins, specifically other Kv channel isoforms, also ignore the perimeter fence, we re-examined the cell surface distribution of YFP-Kv1.4 in HEK cells also expressing CFP-Kv2.1. Our previous work, which indicated that Kv1.4 is both homogeneously distributed and mobile on the HEK cell surface (O'Connell and Tamkun, 2005), suggests that Kv1.4 localization is indifferent to Kv2.1 localization but high resolution imaging of the Kv2.1 clusters on the HEK cell basal surface was not performed. Fig. 5A shows a high magnification view of the HEK cell basal surface, where CFP-Kv2.1-HA clusters often accumulate (Fig. 1) (see also O'Connell and Tamkun, 2005). Comparison of Fig. 5A with 5B indicates that YFP-Kv1.4-myc is expressed at similar densities on both sides of the CFP-Kv2.1-HA cluster perimeters (outlined in white). These results are consistent with the mobile Kv1.4 being indifferent to the Kv2.1 cluster-defining fence.

FRAP experiments were performed next to confirm that Kv1.4 channels ignore the perimeter fence and readily diffuse into the Kv2.1 clusters. As illustrated in Fig. 5C, YFP-Kv1.4-myc channels in a region of concentrated CFP-Kv2.1-HA clusters were photobleached. Fluorescence recovery then occurred evenly throughout the Kv2.1 clusters as predicted if Kv1.4 diffusion is indifferent to the cluster perimeter (Fig. 5D). The FRAP time course shown in Fig. 5E was used to estimate a YFP-Kv1.4-myc diffusion coefficient of 0.2 μm^2/second for this example. Overall, the mean diffusion coefficient for YFP-Kv1.4-myc was 0.28±0.13 μm^2/second, n=11. This value is significantly larger than the 0.08±0.03 μm^2/second calculated for the non-clustered Kv2.1, P<0.001. Movie 1 in

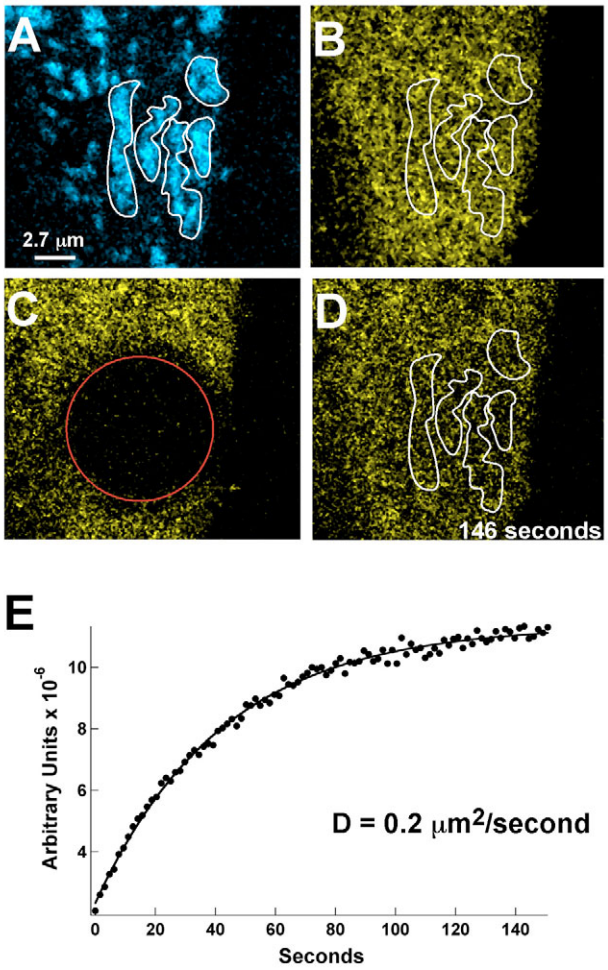

Fig. 5. Detection of Kv1.4 within the Kv2.1 cell surface cluster. FRAP analysis of YFP-Kv1.4-myc mobility. HEK cells expressing both CFP-Kv2.1-HA and YFP-Kv1.4-myc were imaged for each fluorophore. (A) Localization of CFP-Kv2.1-HA. (B) Homogeneous distribution of YFP-Kv1.4-myc. Note that Kv1.4 is present at the same cell surface density on both sides of the Kv2.1 cluster perimeter (outlined in white). (C) Photobleach of YFP-Kv1.4-myc contained within the red ROI. This field of view is identical to that presented in A and B. (D) YFP fluorescence recovery at 146 seconds, illustrating that the mobile YFP-Kv1.4-myc channels have diffused into the CFP-Kv2.1-HA clusters outlined in white. (E) Time course of fluorescence recovery within the bleach ROI, illustrating a FRAP time constant of 42.4 seconds in this representative experiment. Using this value, we calculated that the mobile YFP-Kv1.4-myc channels in this cell have a diffusion coefficient of 0.2 μm^2/second. The mean diffusion coefficient for YFP-Kv1.4-myc was 0.28±0.13 μm^2/second, n=11. Cells were imaged every 1.6 seconds.

supplementary material illustrates the FRAP time course summarized in Fig. 5C,D.

Non-clustered GFP-Kv2.1 channels can become trapped after crossing the cluster perimeter

A third, but relatively rare, type of Qdot GFP-Kv2.1-loopBAD track was one in which a channel either exited the surface cluster after being tracked for 2-5 minutes or a non-clustered channel diffused across a cluster perimeter and then became trapped. Only nine instances of this nature were recorded; five

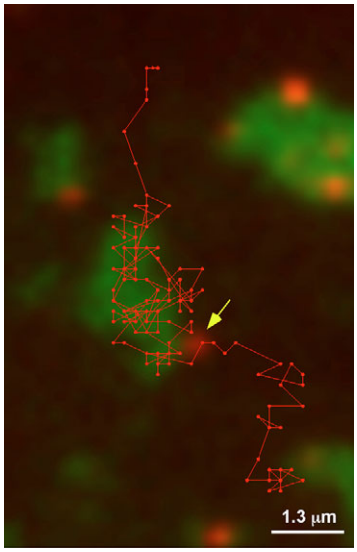

Fig. 6. Non-clustered GFP-Kv2.1-loopBAD channels can become trapped after crossing the cluster perimeter. Illustrated is a Qdot655-tagged channel entering a cluster (yellow arrow) and being transiently retained within the cluster perimeter for 112 seconds before escaping. Cluster perimeter crossing events were relatively rare, being observed in only 9 out of more than 80 Qdot tracks analyzed. See supplementary material Movie 2. The Qdot was imaged every 0.8 seconds.

tracks showed a channel leaving a cluster and four tracks were recorded where a non-clustered channel entered a cluster. Within this latter group, two individual examples were recorded where a channel entered a cluster, was trapped there for approximately 2 minutes, and then escaped. One such track is illustrated in Fig. 6. Here the non-clustered channel was tracked for 27 seconds before it entered a nearby cluster where it was retained for 110 seconds before exiting. The video sequence of this track is shown in supplementary material Movie 2. In this movie it is apparent the mobile Qdot never ranges beyond the GFP-Kv2.1-loopBAD-defined cluster perimeter once it enters the cluster. One possibility is that the Kv2.1 channel is modified once it enters the surface cluster and this modification then renders the channel sensitive to the perimeter fence. Loss of this modification then allows escape from the cluster.

Relationship between the cortical actin cytoskeleton and Kv2.1-containing surface clusters

Cortical actin has been implicated in the transient restriction of membrane protein diffusion and in the division of the cell surface into various microdomains (Kusumi et al., 2005; Suzuki et al., 2005). We recently demonstrated that disruption of actin polymerization with latrunculin A (Lat A) increases Kv2.1 cluster size more than fourfold in both HEK cells and hippocampal neurons (O'Connell et al., 2006), suggesting a relationship between cortical actin and Kv2.1 cluster formation and/or maintenance. However, because an altered cytoskeleton may indirectly affect many cell signaling mechanisms, we next sought to determine whether a direct relationship exists between the cluster perimeter and cortical actin.

Fig. 7 illustrates the relationship between actin filaments, as

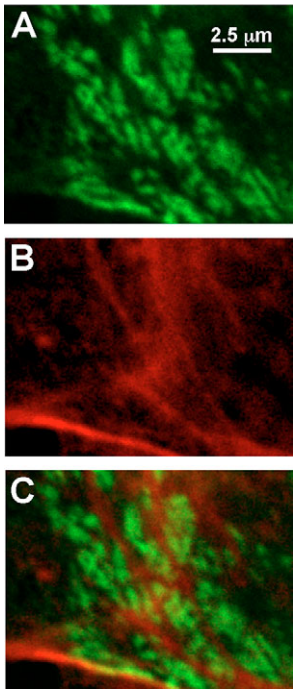

Fig. 7. Phalloidin-stained actin filaments direct Kv2.1 surface cluster orientation. HEK cells expressing GFP-Kv2.1-loopBAD were formaldehyde fixed, permeabilized with Triton X-100 and stained with Alexa Fluor 594-labeled phalloidin. (A) GFP-Kv2.1-loopBAD expression pattern. (B) Phalloidin pattern. (C) The overlay of panels A and B.

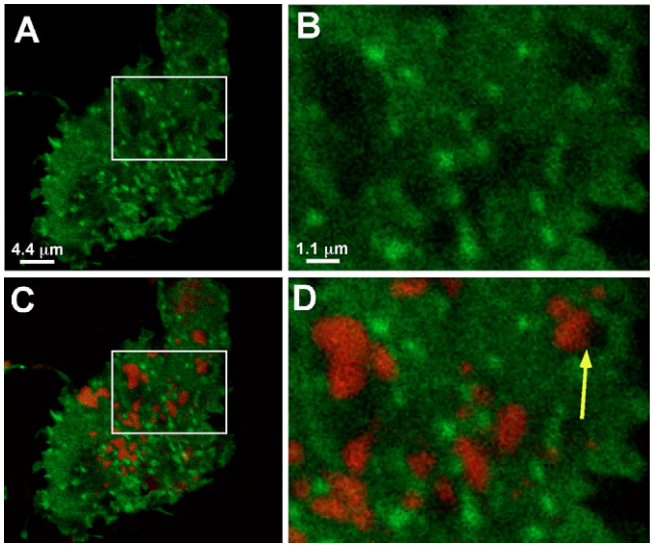

Fig. 8. Kv2.1 surface clusters correlate with an absence of cortical actin. HEK cells were co-transfected with mCherry-Kv2.1-loopBAD and GFP-actin and imaged without fixation. (A) The expression pattern of GFP-actin. (C) Localization of mCherry-Kv2.1-loopBAD overlaid with GFP-actin expression. (B,D) Enlargements of the boxed regions in A and C. The yellow arrow in D indicates that the Kv2.1 cluster perimeter did not always align with the border of the actin-free zone. Nonetheless, Kv2.1 clusters tend to form where actin is reduced.

detected via Alexa Fluor 594-labelled phalloidin staining and GFP-Kv2.1-loopBAD clusters in formaldehyde-fixed HEK cells. Although HEK cells lack an extensive f-actin-based stress fiber network (Davies et al., 2006), large actin filaments were occasionally detected near Kv2.1 surface clusters. The Kv2.1 clusters appeared to align themselves alongside the actin filaments even though significant phalloidin staining never colocalized with the Kv2.1 clusters.

We also co-expressed mCherry-Kv2.1-loopBAD with GFP-actin to examine the relationship between Kv2.1 surface localization and actin in living cells. Fig. 8 illustrates the relationship between the mCherry-Kv2.1-loopBAD-containing clusters and the GFP-actin. Comparison of Fig. 8B with Fig. 8D confirms an inverse relationship between the GFP-actin and the Kv2.1 clusters, with the clusters preferring regions with relatively little cortical actin. As indicated by the yellow arrow in Fig. 8D, there was not always an exact relationship between the edge of the Kv2.1 cluster and the GFP-actin border. Thus, it is likely that cortical structures, in addition to f-actin, function to form the cluster perimeter fence.

Although our interpretation of the data in Fig. 8 is that Kv2.1 clusters reside within cortical actin wells, it is possible that altered membrane structure, e.g. membrane ruffling outside the clusters, artifactually gave rise to the appearance of increased actin outside the clusters. To test this possibility, we visualized the membrane with DiI (1,1′-dioctadecyl-3,3,3′,3′-tetramethylindocarbocyanine perchlorate) staining as shown in supplementary material Fig. S1. DiI incorporation was homogenous over the plasma membrane region containing the surface clusters, making it unlikely that membrane ruffling is responsible for the inverse correlation between the clusters and actin. Note also that the homogenous distribution of Kv1.4 over the cell surface, both inside and outside of the cluster as shown in Fig. 5, also argues against this type of artifact.

Actin-depolymerization induces Kv2.1 declustering

Given the close relationship between cortical actin and the Kv2.1 clusters illustrated in Figs 7 and 8, we next re-examined the effects of actin depolymerization on cluster maintenance. The latrunculin A we used previously (O'Connell et al., 2006) alters the actin cytoskeleton via its G-actin-binding activity (Coue et al., 1987). This agent, although favoring actin depolymerization via G-actin sequestration, does not directly sever actin filaments. By contrast, toxins such as swinholide A both sequester G-actin and sever F-actin, thus being more effective at actin cytoskeletal disruption (Bubb et al., 1995). Therefore, we investigated how this more aggressive actin disruptor would alter the Kv2.1-containing surface clusters. As illustrated in Fig. 9A,B, 75 nM swinholide A had basically the same effect as latrunculin A (O'Connell et al., 2006): cluster number decreased with a corresponding increase in size. Thus, the number of channels within the cluster did not significantly change. Overall, application of 75 nM swinholide A for 30-40 minutes caused the cluster number to drop to 50±26% of that observed before treatment. There was a corresponding 190±36% increase in mean cluster area with no significant change in clustered GFP-Kv2.1 content. (P values for these parameters were 0.04, <0.001 and 0.8, respectively, relative to the solvent control, n=6.) Raising the swinholide concentration to 200 nM caused the clusters to decrease in both number and

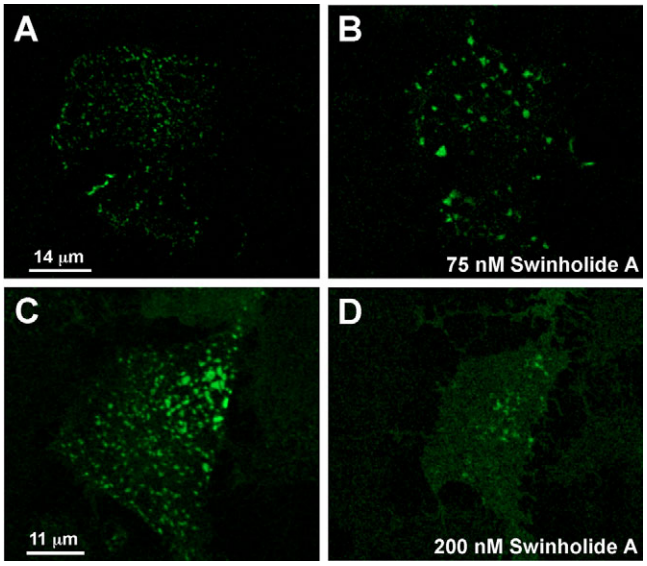

Fig. 9. Concentration-dependent effects of swinholide A on GFP-Kv2.1-HA cluster size. The effect of 75 or 200 nM swinholide A on Kv2.1 cluster size was determined as illustrated in panels A and B, or C and D, respectively. (A,C) Cluster distribution on the bottom of the cell before either 75 or 200 nM swinholide treatment, respectively. (B,D) The cluster pattern 40 minutes later. In this example, 75 nM swinholide reduced the cluster number from 284 to 123 while increasing the average size from 0.34 to 0.50 μm^2. There was a 1.2-fold increase in the GFP signal associated with the clusters. With the 200 nm concentration, the cluster number decreased from 485 to 113, with the average cluster area decreasing from 0.58 to 0.27 μm^2. The total GFP signal that was cluster associated dropped to 3.5% of its original value.

size along with a dramatic increase in the amount of GFP-Kv2.1 fluorescence not localized within clusters as illustrated in Fig. 9C,D. The clusters effectively dissolved under these conditions. Forty minutes in 200 nM swinholide A decreased cluster number to 45±37% of the starting number, reduced the average size to 34±19% and resulted in only 18% of the channel remaining in any size cluster. (*P* values for these parameters were 0.02, <0.001 and <0.001, respectively, relative to the solvent control, *n*=8.) Fig. S2 in the supplementary material illustrates the morphological changes occurring in the HEK cells as a function of swinholide A addition. Similar changes in cell appearance were observed with concentrations ranging from 75-200 nM. A time course of the swinholide A-induced cluster dissolution is shown in supplementary material Movie 3. A control time series, where the cells received only the DMSO vehicle, is shown in supplementary material Movie 4. This movie illustrates the dynamic nature of the Kv2.1-containing surface clusters that none-the-less remained fairly constant in number and size over the 40 minute imaging period.

Discussion

The regulated localization of Kv channels is crucial for local control of electrical excitability, possibly placing the channels in proximity to local signaling pathways that modulate channel activity and/or cell surface expression. Kv2.1-containing surface clusters are unique membrane structures found in hippocampal neurons in situ (Misonou et al., 2005a), cultured hippocampal neurons (O'Connell et al., 2006) and transfected HEK cells (O'Connell et al., 2006). Such clusters are likely to be linked directly to excitable membrane physiology because they are regulated by both neuronal-activity-induced Ca^{2+} influx and Ca^{2+} release from internal stores, the latter being activated by both hypoxia and chemically induced ischemia (Misonou et al., 2005a; Misonou et al., 2004; Mohapatra and Trimmer, 2006).

The Kv2.1-containing clusters are most likely defined by a perimeter fence as opposed to transient tethering to a scaffolding complex

The single-particle-tracking data presented in Fig. 2 indicate that Kv2.1 has similar diffusion coefficients on both sides of the cluster perimeter, 0.03±0.02 μm^2/second inside the cluster and 0.06±0.05 μm^2/second outside. As summarized in Table 1, mobile membrane proteins such as extra-synaptic neurotransmitter receptors have reported diffusion coefficients of 0.01-0.45 μm^2/second. Mobile lipids such as GM1 gangliosides have diffusion coefficients of 0.07 μm^2/second (Saxton and Jacobson, 1997). By contrast, clustered membrane proteins commonly believed to be tethered to scaffolding proteins, e.g. synaptic neurotransmitter receptors, have diffusion coefficients that are often two orders of magnitude slower than the non-tethered protein, ranging from 0.0003 to

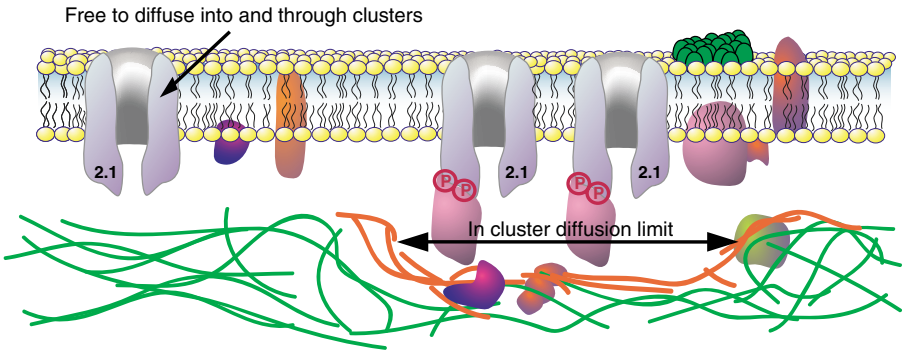

Fig. 10. Proposed model for the Kv2.1-containing cluster perimeter fence showing the clustered Kv2.1 channel trapped in a well within the cortical cytoskeleton. The walls of this well form the functional fence, which retains channels that have sufficient depth owing to their assembly with accessory proteins, perhaps via phosphorylation, at the channel C-terminus. Thus, the channel within the cluster has the same lateral mobility as the non-clustered channel but remains corralled. Other membrane proteins, and non-modified Kv2.1 channels, do not have the depth to be trapped within the well. Cortical actin, illustrated in green, is proposed to play a role in separating and organizing the clusters as opposed to actually being the fence itself. Unknown cytoskeletal elements, illustrated in orange, are proposed to form the actual cortical well. Alternatively, the orange color might represent stable actin filaments that are poorly labeled by GFP-actin but severed by high swinholide A concentrations.

Table 1. Summary of cell surface diffusion quantified by single particle tracking

Membrane protein	Cell type	Diffusion coefficient (μm^2/second)	Reference
Kv2.1			
Wild-type within cluster*	HEK cells	0.03±0.02	This report
Wild-type outside cluster*	HEK cells	0.06±0.05	This report
C-terminus mutant (nonclustering)*	HEK cells	0.07±0.04	This report
Synaptic NT receptors			
Glycine receptors, synaptic*,†	Neurons	0.001-0.003	Dahan et al., 2003; Meier et al., 2001
AMPA receptors, synaptic‡	Neurons	<0.007	Tardin et al., 2003
Extrasynaptic NT receptors			
Glycine receptors, extrasynaptic*,†	Neurons	0.01-0.02	Dahan et al., 2003; Meier et al., 2001
AMPA receptors, extrasynaptic‡	Neurons	0.45	Tardin et al., 2003
Immobile membrane proteins			
E-cadherin§	Epidermal cells	0.0016	Kusumi et al., 1993
Transferrin receptor§	Fibroblasts	0.0024	Sako and Kusumi, 1995
GABA receptors¶	COS cells	0.0003	Peran et al., 2001
Mobile membrane proteins			
Transferrin receptor§	Fibroblasts	0.1	Sako and Kusumi, 1995
Thy 1 (GPI-linked)§	C3H fibroblasts	0.072	Saxton and Jacobson, 1997
GABA receptors¶	COS cells	0.04	Peran et al., 2001
Lipid			
GM-1 ganglioside§	Fibroblasts	0.07	Saxton and Jacobson, 1997

*Qdot tracking; †antibody-coated 0.5 μm latex beads; ‡Cy5 or Alexa-Fluor-647-labeled antibodies; §40-nm-gold-conjugated antibodies; ¶antibody-coupled 50-100 nm fluorescent spheres.

0.003 μm^2/second. All of these diffusion coefficients were measured using the single-particle-tracking approach used in our present work [for a detailed review of this technology see Kusumi et al. (Kusumi et al., 2005)]. Thus, only a twofold difference in mean Kv2.1 mobility between clustered and non-clustered Kv2.1 strongly argues against Kv2.1 cluster formation being driven by sub-membrane scaffolding complexes. In addition, we have several instances where the Kv2.1 diffusion coefficient within a cluster was greater than the diffusion coefficients of non-clustered channels in the same cell (data not shown).

Although the mean Kv2.1 diffusion coefficient within the clusters is twofold slower than that measured outside the perimeter fence (P=0.01 in the non-paired t-test), it is likely that this difference arises from trying to compare diffusion in a restricted compartment with that observed in a barrier-free environment. Diffusion of channels within the cluster should be somewhat underestimated owing to collisions with the perimeter fence, because the clusters are 1-3 μm in diameter and the velocities of the tracked quantum dots range from 0.3-0.6 μm/second. Given that our highest Qdot imaging rate was 2 Hz, diffusion-limiting collisions with the fence are expected within the clusters. Although a greater rate of data acquisition is not possible with our current procedures and equipment, we predict that acquisition rates of 50-100 Hz would produce identical diffusion coefficients on both sides of the cluster fence.

The cluster perimeter fence controls the diffusion of only the Kv2.1 channels it corrals

The perimeter fence probably regulates the lateral diffusion of only selected membrane proteins. Non-clustered channels such as Kv1.4, which are homogeneously distributed over the cell surface, are indifferent to where the Kv2.1 microdomains are located, as indicated in Fig. 5. As illustrated in Figs 2 and 4, Kv2.1 channels outside the surface clusters readily diffused across the cluster perimeter as if it did not exist. On rare occasions (4 of >35 nonclustered channel tracks analyzed), we recorded a freely diffusing channel entering a cluster and then becoming trapped as illustrated in Fig. 6. The simplest explanation for this trapping phenomenon is that upon cluster entry a modification occurred that rendered the channel sensitive to the fence perimeter. In two of these cases, the newly trapped channel was only transiently retained, escaping after about 2 minutes of confinement. Although transient breakdown of the perimeter fence could be responsible for such escape behavior, this mechanism seems unlikely given that channel retention within the clusters, as measured by stable GFP content and single-channel dwell times exceeding 25 minutes, is extremely long-lived with a half-life probably measured in hours. It is more likely that the modification that rendered the channel susceptible to the perimeter fence was lost, thus allowing the channel to escape. However, long-term cluster stability is probably maintained by constant steady state diffusion, escape and entry across the perimeter fence.

The Kv2.1 surface clusters may be formed by wells in the cortical cytoskeleton

Since cortical actin has been implicated in restricting the lateral diffusion of membrane proteins, our earliest ideas were that the Kv2.1 cluster perimeter was composed of actin and that actin depolymerization would induce cluster fragmentation. However, as we showed previously (O'Connell et al., 2006), latrunculin A treatment actually increases cluster size, arguing against a simple actin ring forming the cluster perimeter. Still, the Lat A effect suggests there is some relationship between cortical actin and Kv2.1 cluster formation or maintenance. Therefore, in our present work, we examined the physical relationship between actin and the Kv2.1 clusters and the effect of stronger actin-depolymerizing agents. As shown in Fig. 7, although actin filaments appear to have an organizing influence on the Kv2.1 clusters, the clusters themselves prefer cell surface regions not associated with phalloidin-positive f-actin. The observation that Kv2.1 clusters are seen most often where

GFP-actin is the lowest (Fig. 8), is also consistent with cluster structure and localization being related to the arrangement of cortical actin. The simplest idea is that the clusters are formed within depressions of the cortical cytoskeleton.

The dose-dependent effects of swinholide A on the Kv2.1 clusters (Fig. 9) also support a role for the actin cytoskeleton in cluster maintenance. It is intriguing that swinholide A has dose-dependent effects, inducing cluster fusion at lower concentrations in a manner similar to latrunculin A (O'Connell et al., 2006) but at greater concentrations causing cluster dissolution. This dose response is not surprising given that swinholide A not only binds G-actin to block polymerization but also severs F-actin. The severing activity probably requires a higher concentration since the filaments are likely to bind multiple swinholide molecules before fragmentation occurs (Bubb et al., 1995). This severing is probably what actually causes the Kv2.1 cluster dissolution. Taken together, these data suggest that f-actin pools with distinct turnover rates are involved in cluster maintenance. Filaments with more rapid turnover should be sensitive to both latrunculin A and lower concentrations of swinholide A. These filaments may play a primary role in maintaining cluster separation. The more stable f-actin is affected only at the higher swinholide A concentration that induces filament severing. These stable filaments may be more directly involved in forming the cluster perimeter itself.

Proposed model for the Kv2.1 surface cluster

Any model attempting to describe the mechanism by which Kv2.1 channels are retained within the cell surface microdomains must explain the following experimental observations. (1) Kv1.4 is equally distributed across the Kv2.1 cluster perimeter (Fig. 5); (2) non-clustered Kv2.1 can readily cross the fence as determined by FRAP and single-particle-tracking analysis (Figs 2 and 4); (3) single-particle tracking indicates that nonclustered channels can become trapped within the cluster following entry (Fig. 6); (4) once clusters collide they actually fuse and exchange Kv2.1 channels (O'Connell et al., 2006); (5) channels corralled within the cluster have a mobility similar to that of channels outside the cluster (Fig. 2); (6) there is an inverse relationship between the actin components of the cortical cytoskeleton and the Kv2.1-containing clusters (Figs 7 and 8); and (7) decreased actin polymerization results in either increased cluster size (O'Connell et al., 2006) or complete cluster dissolution (Fig. 9, supplementary material Movie 3).

The model presented in Fig. 10 accommodates all of these experimental observations. Here the side of a well or depression in the cortical cytoskeleton forms the actual fence. Kv2.1 channels within the cluster are proposed to interact with accessory proteins via the C-termini in a phosphorylation-dependent manner. This added mass increases the channel extension into the cytoplasm and thus causes collisions with the cluster-forming wall or cortical fence. Given the inexact relationship between the cluster perimeter and the GFP-actin (see the yellow arrow in Fig. 8D), it is possible that unknown structural elements exist between the cortical f-actin and the true cluster perimeter. Non-clustered Kv2.1 channels, and channels such as Kv1.4, do not bind the accessory proteins and thus are free to readily diffuse into, and through, the Kv2.1 cluster. The Kv2.1 C-terminus is strongly implicated in this process because its deletion abolishes Kv2.1 clustering (Fig. 3) (see also Lim et al., 2000). In addition, gain-of-function experiments indicate that transfer of the Kv2.1 C-terminus onto non-clustering Kv channels such as Kv1.5, induces Kv1.5 cluster formation in HEK cells (Mohapatra and Trimmer, 2006). Since Kv2.1 does not form surface clusters in all cell types, it is likely that there is either cell-specific expression of Kv2.1 C-terminal-binding proteins or a cell-specific cytoskeleton.

Kusumi and co-workers have recently performed a detailed structural analysis by electron tomography of cytoskeletal components in rat kidney fibroblasts and keratinocytes that are likely to restrict the lateral diffusion of membrane proteins (Morone et al., 2006). Here, some of the actin filaments are within 10.2 nm of the cytoplasmic surface of the plasma membrane where they are proposed to form the boundaries of membrane compartments responsible for the temporary confinement of membrane molecules with regard to their lateral diffusion. These compartments are smaller (at most 0.1 μm in diameter) than the Kv2.1 cell surface clusters and residence times are measured in milliseconds as opposed to minutes (Kusumi et al., 2005; Morone et al., 2006). All cells probably have such cytoskeletal compartments just under the cell surface that influence the lateral diffusion of membrane proteins. The Kv2.1 clusters under study in our work might represent the most extreme example of the cortical cytoskeleton influence over membrane protein diffusion.

It is commonly assumed that ion channel localization must involve static tethering to scaffolding proteins that in turn are linked directly to the cytoskeleton. The data presented here strongly suggest that mobile Kv2.1 channels are corralled behind a fence that is part of the cortical cytoskeleton. This sub-membrane fence is selective towards only the confined channels. The Kv2.1-containing surface clusters represent a new mechanism for the stable localization of ion channel proteins to specific cell surface domains.

Materials and Methods

Preparation of expression vectors and cell transfection.

The construction of vectors containing GFP-Kv2.1-HA, GFP-Kv2.1-loopBAD, CFP-Kv2.1-HA and YPF-Kv1.4-myc has been described previously (O'Connell et al., 2006; O'Connell and Tamkun, 2005). The GFP-Kv2.1-loopBAD contains the biotin acceptor peptide sequence (GGGAGGLVGLNDIFEAQ**K**IEWHEAR-GGGAGG, boldfaced lysine is biotinylated, underlined sequence represents inserted amino acids not part of the actual biotin acceptor peptide) for biotin ligase inserted into the extracellular loop between S1 and S2 (Howarth et al., 2005; O'Connell et al., 2006). mCherry was obtained from DNA 2.0 and attached to the Kv2.1 N-terminus in the same position as GFP. GFP-actin was obtained from Clontech.

The expression vectors (0.5-3 μg per confluent 100 mm dish) were electroporated into HEK293 cells (ATCC, Manassas, VA) using a Bio-Rad Genepulser Xcell (Bio-Rad Laboratories, Hercules, CA). Electroporation was done using a single pulse of 110 V for 25 milliseconds in a 0.2 cm gap cuvette. Cells were then plated onto Matrigel-coated glass-bottom 35 mm dishes (Mat-Tek, Ashland, MA) in DMEM + 10% fetal bovine serum and used within 24 hours of electroporation.

Live cell confocal imaging

HEK cells expressing GFP-tagged Kv2.1 constructs were most often imaged using an Olympus FV1000 confocal microscope equipped with spectral detectors and the SIM scanner. GFP was excited using the 488 nm line of an Ar laser set at 0.1-0.5% transmission and emission collected using the variable bandpass filter set at 500-550 nm. A 60×, 1.4 NA oil-immersion objective was used for imaging and the pinhole diameter set for 1 Airy Unit. For each image, the detector voltage was adjusted as necessary to utilize the full 12-bit linear range. For the imaging of individual Kv2.1-containing clusters, an optical zoom of 8-15× was often used. Images were acquired every 0.5-5 seconds as indicated at 512×512 resolution. The 655 quantum dots used to monitor single channel diffusion were imaged with the

633 laser line at 100% transmission and the LP650 filter based PMT on the FV1000 at 320×320 resolution. For imaging of 605 quantum dots bound to GFP-Kv2.1-loopBAD, a DeltaVision RT wide field microscope system was used with a 100× 1.4 NA objective and filter sets optimized for FITC and Rhodamine. Image exposure was 10 milliseconds for the green channel and 200 milliseconds for the red using a CoolSnap HQ camera at 3×3 binning. Imaging with both systems was performed in HEPES-buffered saline containing: 146 mM NaCl, 4.7 mM KCl, 2.5 mM $CaCl_2$, 0.6 mM $MgSO_4$, 1.6 mM $NaHCO_3$, 0.15 mM NaH_2PO_4, 0.1 mM ascorbic acid, 8 mM glucose and 20 mM HEPES, pH 7.4 (imaging saline). For all imaging experiments, the stage and objective were heated to 37°C. Cells were imaged for less than 1 hour on the microscope stage. However, no changes in the Kv2.1 surface expression were observed after up to 4 hours in imaging saline at 37°C. Long-term imaging under the conditions described above did not alter the expression pattern.

Offline image analysis was done using the Olympus FV1000 software (version 1.03) and Volocity 4.0.1 (Improvision, Lexington, MA). Data analysis and curve fitting was performed with SigmaPlot 8 (Systat, Point Richmond, CA) or IgorPro 5.03 (Wavemetrics, Portland, OR). Images were filtered in Volocity using a 3×3 median filter.

Quantum-dot-based single-channel tracking

For the single particle tracking of cell surface Kv2.1, GFP-Kv2.1-loopBAD was expressed in HEK cells and biotinylated as previously described using bacterially synthesized BirA (Howarth et al., 2005; O'Connell et al., 2006). The live cells were then incubated for 10 minutes with a 1:10,000 dilution of streptavidin-coated quantum dots (either QD605 or QD655 from Invitrogen) in imaging saline containing 1% BSA (IgG- and fatty-acid-free). The cells were then rinsed extensively with imaging saline + 1 mM biotin to guard against streptavidin-induced channel crosslinking and imaged as described above. Controls for nonspecific quantum dot (Qdot) binding included imaging cells expressing GFP-Kv2.1-HA that had been carried through the entire labeling protocol or using cells expressing GFP-Kv2.1-loopBAD that were not incubated with the BirA biotin ligase. Although imaging individual quantum dots immobilized onto a glass coverslip confirmed that single dots were tracked in the transfected cells, we cannot guarantee that a single dot is tethered to a single channel in our imaging experiments.

MSD analysis of single particle movement

Qdot tracks were plotted and analyzed using Volocity (v3.6.1 and v4.0.1) (Improvision, Lexington MA). Given the 'blinking' behavior of Qdots, the tracking was done manually. The *x*-*y* coordinates of individual tracks were imported into SigmaPlot 8 for analysis of MSD according to Eqn 1 (Hao et al., 2005).

$$MSD(n\delta t) = \frac{1}{N-n}\sum_{j=1}^{N-n}\{[x(j\delta t + n\delta t) - x(j\delta t)]^2 + [y(j\delta t + n\delta t) - y(j\delta t)]^2\}\,, \quad (1)$$

where t is the time interval at which images were taken, $x(t)$ and $y(t)$ are the coordinates of a Qdot at time t, and N is the total number of images in a recording. n and j are positive integers with n=1,2,…,(N-1). Movement over a period corresponding to 10% of the total images acquired (0.1$N$$t$) was quantified as described by Kusumi and co-workers (Kusumi et al., 1993). The apparent diffusion coefficient was calculated as one-fourth of the slope of the linear regression line fitted to the n=2 to 10 values of the MSD(ndt) [MSD(ndt)=4D(t) + c].

FRAP analysis of Kv channel diffusion

For FRAP analysis of GFP-Kv2.1, a circular region of interest (ROI) was photobleached using the SIM scanner of the Olympus FV1000 in tornado scan mode with a 405 nm diode laser at 12-20% transmission for 0.5-1 seconds as previously described (O'Connell et al., 2006; O'Connell and Tamkun, 2005). The SIM scanner was synchronized with the main scanner during bleach and acquisition. Following bleach, imaging was performed by raster scanning with the 488 nm line of a 40 mW Ar laser at 0.2-0.5% transmission. The variable bandpass filter was set to detect 505-530 nm emission and images were acquired every 0.5-1.1 seconds at 512×512 resolution. For YFP-Kv1.4-myc, a circular ROI was photobleached using the main scan head and the 515 nm laser at 100% transmission for 2 seconds. The recovery was then monitored with this laser set to 0.2-0.5% transmission. Images were acquired every 1.5 seconds at 640×640 resolution.

Fluorescence intensity, in arbitrary units, within the bleach ROI was fit according to Eqn 2 as previously described (O'Connell and Tamkun, 2005) and the macroscopic diffusion coefficient (D) determined from the $T_{½}$ according to Eqn 3 and Eqn 4 and the approach of Axelrod (Axelrod et al., 1976).

$$f(x) = \sum_{i=1}^{n} A_i(1-e^{(-t/\tau_i)})\,, \quad (2)$$

where A_i is the amplitude of each component, t is time and τ_i is the time constant of each component.

$$T_{½} = \tau\,(\ln 2), \quad (3)$$

where τ equals the time constant from Eqn 2.

$$D = 0.88(r^2/4T_{½}), \quad (4)$$

where D is the diffusion coefficient, r is the radius in μm of the bleached ROI and $T_{½}$ is the half-life from Eqn 3.

Phalloidin staining of actin filaments

HEK cells transfected with GFP-Kv2.1-loopBAD were fixed with 4% formaldehyde in PBS for 5 minutes at room temperature. The cells were then incubated in 10% goat serum in PBS for 20 minutes followed by 20 minutes in 1% BSA in PBS. Actin filaments were labeled with Alexa Fluor 594-phalloidin (Invitrogen) diluted 1:40 in 1% BSA in PBS for 15 minutes. After three brief rinses in PBS, the cells were embedded in AquaPolymount (Polysciences), covered with a coverslip and imaged.

Statistical analysis

Mean values ± s.d. are presented. Significance was assessed using the non-paired *t*-test.

The authors thank Kathy Partin and Scott Earley for comments on the manuscript. This work was supported by NIH RO1 grants NS41542 and HL49330 and NIH NRSA F32 HL77056 and K99 HL087591 to M.M.T. and K.M.S.O., respectively.

References

Antonucci, D. E., Lim, S. T., Vassanelli, S. and Trimmer, J. S. (2001). Dynamic localization and clustering of dendritic Kv2.1 voltage-dependent potassium channels in developing hippocampal neurons. *Neuroscience* **108**, 69-81.

Axelrod, D., Koppel, D. E., Schlessinger, J., Elson, E. and Webb, W. W. (1976). Mobility measurement by analysis of fluorescence photobleaching recovery kinetics. *Biophys. J.* **16**, 1055-1069.

Bubb, M. R., Spector, I., Bershadsky, A. D. and Korn, E. D. (1995). Swinholide A is a microfilament disrupting marine toxin that stabilizes actin dimers and severs actin filaments. *J. Biol. Chem.* **270**, 3463-3466.

Coppock, E. A., Martens, J. R. and Tamkun, M. M. (2001). Molecular basis of hypoxia-induced pulmonary vasoconstriction: role of voltage-gated K(+) channels. *Am. J. Physiol. Lung Cell. Mol. Physiol.* **281**, L1-L12.

Coue, M., Brenner, S. L., Spector, I. and Korn, E. D. (1987). Inhibition of actin polymerization by latrunculin A. *FEBS Lett.* **213**, 316-318.

Dahan, M., Levi, S., Luccardini, C., Rostaing, P., Riveau, B. and Triller, A. (2003). Diffusion dynamics of glycine receptors revealed by single-quantum dot tracking. *Science* **302**, 442-445.

Davies, S. L., Gibbons, C. E., Vizard, T. and Ward, D. T. (2006). Ca^{2+}-sensing receptor induces Rho kinase-mediated actin stress fiber assembly and altered cell morphology, but not in response to aromatic amino acids. *Am. J. Physiol. Cell Physiol.* **290**, C1543-C1551.

Du, J., Tao-Cheng, J. H., Zerfas, P. and McBain, C. J. (1998). The K^+ channel, Kv2.1, is apposed to astrocytic processes and is associated with inhibitory postsynaptic membranes in hippocampal and cortical principal neurons and inhibitory interneurons. *Neuroscience* **84**, 37-48.

Du, J., Haak, L. L., Phillips-Tansey, E., Russell, J. T. and McBain, C. J. (2000). Frequency-dependent regulation of rat hippocampal somato-dendritic excitability by the K^+ channel subunit Kv2.1. *J. Physiol.* **522**, 19-31.

Hao, M., Li, X., Rizzo, M. A., Rocheleau, J. V., Dawant, B. M. and Piston, D. W. (2005). Regulation of two insulin granule populations within the reserve pool by distinct calcium sources. *J. Cell Sci.* **118**, 5873-5884.

Howarth, M., Takao, K., Hayashi, Y. and Ting, A. Y. (2005). Targeting quantum dots to surface proteins in living cells with biotin ligase. *Proc. Natl. Acad. Sci. USA* **102**, 7583-7588.

Kusumi, A., Sako, Y. and Yamamoto, M. (1993). Confined lateral diffusion of membrane receptors as studied by single particle tracking (nanovid microscopy). Effects of calcium-induced differentiation in cultured epithelial cells. *Biophys. J.* **65**, 2021-2040.

Kusumi, A., Nakada, C., Ritchie, K., Murase, K., Suzuki, K., Murakoshi, H., Kasai, R. S., Kondo, J. and Fujiwara, T. (2005). Paradigm shift of the plasma membrane concept from the two-dimensional continuum fluid to the partitioned fluid: high-speed single-molecule tracking of membrane molecules. *Annu. Rev. Biophys. Biomol. Struct.* **34**, 351-378.

Kwik, J., Boyle, S., Fooksman, D., Margolis, L., Sheetz, M. P. and Edidin, M. (2003). Membrane cholesterol, lateral mobility, and the phosphatidylinositol 4,5-bisphosphate-dependent organization of cell actin. *Proc. Natl. Acad. Sci. USA* **100**, 13964-13969.

Lim, S. T., Antonucci, D. E., Scannevin, R. H. and Trimmer, J. S. (2000). A novel targeting signal for proximal clustering of the Kv2.1 K^+ channel in hippocampal neurons. *Neuron* **25**, 385-397.

Meier, J., Vannier, C., Serge, A., Triller, A. and Choquet, D. (2001). Fast and reversible trapping of surface glycine receptors by gephyrin. *Nat. Neurosci.* **4**, 253-260.

Misonou, H., Mohapatra, D. P., Park, E. W., Leung, V., Zhen, D., Misonou, K., Anderson, A. E. and Trimmer, J. S. (2004). Regulation of ion channel localization and phosphorylation by neuronal activity. *Nat. Neurosci.* **7**, 711-718.

Misonou, H., Mohapatra, D. P., Menegola, M. and Trimmer, J. S. (2005a). Calcium- and metabolic state-dependent modulation of the voltage-dependent Kv2.1 channel regulates neuronal excitability in response to ischemia. *J. Neurosci.* **25**, 11184-11193.

Misonou, H., Mohapatra, D. P. and Trimmer, J. S. (2005b). Kv2.1: a voltage-gated K(+) channel critical to dynamic control of neuronal excitability. *Neurotoxicology* **26**, 743-752.

Mohapatra, D. P. and Trimmer, J. S. (2006). The Kv2.1 C terminus can autonomously transfer Kv2.1-like phosphorylation-dependent localization, voltage-dependent gating, and muscarinic modulation to diverse Kv channels. *J. Neurosci.* **26**, 685-695.

Morone, N., Fujiwara, T., Murase, K., Kasai, R. S., Ike, H., Yuasa, S., Usukura, J. and Kusumi, A. (2006). Three-dimensional reconstruction of the membrane skeleton at the plasma membrane interface by electron tomography. *J. Cell Biol.* **174**, 851-862.

Nerbonne, J. M. (2000). Molecular basis of functional voltage-gated K^+ channel diversity in the mammalian myocardium. *J. Physiol.* **525**, 285-298.

O'Connell, K. M. and Tamkun, M. M. (2005). Targeting of voltage-gated potassium channel isoforms to distinct cell surface microdomains. *J. Cell Sci.* **118**, 2155-2166.

O'Connell, K. M., Rolig, A. S., Whitesell, J. D. and Tamkun, M. M. (2006). Kv2.1 potassium channels are retained within dynamic cell surface microdomains that are defined by a perimeter fence. *J. Neurosci.* **26**, 9609-9618.

Pal, S., Hartnett, K. A., Nerbonne, J. M., Levitan, E. S. and Aizenman, E. (2003). Mediation of neuronal apoptosis by Kv2.1-encoded potassium channels. *J. Neurosci.* **23**, 4798-4802.

Pal, S. K., Takimoto, K., Aizenman, E. and Levitan, E. S. (2006). Apoptotic surface delivery of K+ channels. *Cell Death Differ.* **13**, 661-667.

Peran, M., Hicks, B. W., Peterson, N. L., Hooper, H. and Salas, R. (2001). Lateral mobility and anchoring of recombinant GABAA receptors depend on subunit composition. *Cell Motil. Cytoskeleton* **50**, 89-100.

Sako, Y. and Kusumi, A. (1995). Barriers for lateral diffusion of transferrin receptor in the plasma membrane as characterized by receptor dragging by laser tweezers: fence versus tether. *J. Cell Biol.* **129**, 1559-1574.

Saxton, M. J. and Jacobson, K. (1997). Single-particle tracking: applications to membrane dynamics. *Annu. Rev. Biophys. Biomol. Struct.* **26**, 373-399.

Scannevin, R. H., Murakoshi, H., Rhodes, K. J. and Trimmer, J. S. (1996). Identification of a cytoplasmic domain important in the polarized expression and clustering of the Kv2.1 K^+ channel. *J. Cell Biol.* **135**, 1619-1632.

Shaw, G., Morse, S., Ararat, M. and Graham, F. L. (2002). Preferential transformation of human neuronal cells by human adenoviruses and the origin of HEK 293 cells. *FASEB J.* **16**, 869-871.

Suzuki, K., Ritchie, K., Kajikawa, E., Fujiwara, T. and Kusumi, A. (2005). Rapid hop diffusion of a G-protein-coupled receptor in the plasma membrane as revealed by single-molecule techniques. *Biophys. J.* **88**, 3659-3680.

Tamarina, N. A., Kuznetsov, A., Fridlyand, L. E. and Philipson, L. H. (2005). Delayed-rectifier (KV2.1) regulation of pancreatic {beta}-cell calcium responses to glucose: inhibitor specificity and modeling. *Am. J. Physiol. Endocrinol. Metab.* **289**, E578-E585.

Tardin, C., Cognet, L., Bats, C., Lounis, B. and Choquet, D. (2003). Direct imaging of lateral movements of AMPA receptors inside synapses. *EMBO J.* **22**, 4656-4665.